RSC Advances

PAPER

View Article Online
View Journal | View Issue

Cite this: *RSC Adv.*, 2025, **15**, 23966

An enzyme-responsive hydrogel functionalized with mesoporous silica nanoparticles for co-delivery of cisplatin and shRNA to overcome chemotherapy resistance in non-small cell lung cancer

Yi Liu, †*[abc] Zheng Zhang,†[a] Huyang Du,[a] Xiangjun Chen,[a] Nan Hu,[ab] Tingting Yu,[ab] Meili Hou[ab] and Xiaolin Yu*[bcd]

Chemoresistance poses a critical challenge in cancer therapy across diverse tumor types, including non-small cell lung cancer (NSCLC), where chemotherapy-induced neuroendocrine differentiation (NED) of tumor cells plays a pivotal role in acquiring treatment resistance. This process significantly reduces chemotherapy efficacy, accelerates tumor progression, and ultimately worsens patient survival outcomes. The complex mechanisms underlying chemoresistance involve multiple factors, including enhanced DNA repair pathways, increased drug efflux capacity, and alterations in gene expression. Additionally, the tumor microenvironment, a dynamic ecosystem surrounding cancer cells, fosters a protective niche that exacerbates chemotherapy resistance. To address this challenge, we propose an innovative nanocomposite hydrogel system for the co-delivery of cisplatin and short hairpin RNA (shRNA) targeting protein arginine methyltransferase 5 (PRMT5), a key gene implicated in drug resistance. This system utilizes polyethyleneimine-modified mesoporous silica nanoparticles, which serve as nanocarriers, encapsulating cisplatin within the mesopores and coating the surface with methacryloylated hyaluronic acid (HA-MA). The design enables tumor microenvironment-responsive drug release, triggered by hyaluronidase enzymes abundant within the tumor, resulting in nanoparticle disassembly and the release of cisplatin. Simultaneously, the delivery of shRNA silences PRMT5 expression, enhancing chemosensitivity. By integrating targeted gene therapy with chemotherapy, this system offers a promising strategy for overcoming chemoresistance in NSCLC. Targeting both cancer cells and their microenvironment, this approach holds potential to transform the treatment of chemotherapy-resistant cancers, advancing more effective and personalized oncological therapies.

Received 8th May 2025
Accepted 2nd July 2025

DOI: 10.1039/d5ra03250d

rsc.li/rsc-advances

1 Introduction

Lung cancer remains the most commonly diagnosed cancer globally, with approximately 2.5 million new cases reported in 2022. It is categorized into two main types: small-cell lung cancer (SCLC) and non-small-cell lung cancer (NSCLC), the latter being the most prevalent, comprising approximately 85% of cases. Most NSCLC patients present with intermediate-to-advanced stages, characterized by a low five-year survival rate. Current treatment modalities for NSCLC include surgery, chemotherapy, radiotherapy, targeted therapy, and immunotherapy. Chemotherapy, in particular, plays a pivotal role in NSCLC treatment. For early-stage patients, adjuvant chemotherapy reduces tumor size, lowers disease staging, and improves cure rates. For advanced-stage patients, chemotherapy can control the growth and spread of the tumor and prolong the survival period of patients to a certain extent. Common chemotherapeutic agents include etoposide (VP16), paclitaxel, and platinum-based compounds such as cisplatin. These drugs can work by binding to DNA, inhibiting mitosis, and disrupting the metabolic process of cancer cells.[1] However, as treatment proceeds, there is often a decrease in therapeutic efficacy as well as progressive failure due to acquired resistance. Mechanisms of chemoresistance in NSCLC include DNA repair, decreased drug concentration, cancer cell metabolism, and pathological phenotypic transformation.[2–4]

[a]*College of Chemical Engineering, Sichuan University of Science & Engineering, Zigong 643000, China. E-mail: yiliu@suse.edu.cn*

[b]*Institute of Precision Medicine, Zigong Academy of Big Data and Artificial Intelligence in Medical Science, Zigong Fourth People's Hospital, Zigong 643000, China. E-mail: yuxiaolincq@hotmail.com*

[c]*Sichuan Clinical Research Center for Clinical Laboratory, Zigong Fourth People's Hospital, Zigong 643000, People's Republic of China*

[d]*Department of Laboratory Medicine, Zigong Fourth People's Hospital, Zigong 643000, People's Republic of China*

† These authors contributed equally to this work.

Emerging evidence implicates PRMT5 as a critical mediator of drug resistance in NSCLC. PRMT5, as a type II arginine methyltransferase, is vital for the growth, proliferation and migration of cancer cells.[5–7] Overexpression of PRMT5 has been shown to be associated with the proliferative and invasive processes of several cancers, including non-small cell lung cancer. Early studies have found that PRMT5 expression is higher in lung cancer tissues than in normal tissues, and inhibition of PRMT5 suppresses the proliferation of non-small cell lung cancer.[8] Moreover, PRMT5 can also regulate cancer progression by interacting with other proteins and signalling pathways. Huang *et al.* showed that PRMT5 is a key class of oncogenic factors that regulate epithelial-mesenchymal transition (EMT) through the EGFR/Akt signalling axis, and silencing of PRMT5 can affect EMT-related markers at both mRNA and protein levels.[9] Zhang *et al.* pointed out that inhibition of PRMT5 by shRNA down-regulation or by the specific inhibitor GSK591 significantly suppressed the expression of cell cycle protein E1 and cell cycle protein D1 and cell proliferation, and PRMT5 could promote human lung cancer cell proliferation through direct interaction with Akt and regulation of Akt activity.[10] Moreover, PRMT5 upregulates the protein level of the anti-apoptotic protein CFLAR thereby inhibiting apoptosis caused by chemotherapy.[11] Zhou *et al.* found that down-regulation or pharmacological inhibition of PRMT5 reduced the expression of oncogenic factor KLF5 and its downstream targets *in vitro* and *in vivo* thereby promoting the maintenance and proliferation of lung cancer cells.[12] These results suggest that targeting the PRMT5/KLF5 axis may be a potential therapeutic strategy for lung cancer. In addition to this, PRMT5 can influence processes by regulating the cell cycle. It was found that PRMT5 and pICln can cooperate as major epigenetic activators of DNA damage response (DDR) genes, acting to upregulate gene expression. These include genes associated with G2 blockade. In contrast to the role of PRMT5 as an epigenetic repressor. By targeting PRMT5 or pICln, DSB repair can be blocked in a variety of cancer cell lines. Therefore, targeting PRMT5 or pICln in combination with radiotherapy or chemotherapy may be used for cancer treatment.[13] In order to resist chemotherapy, cancer cells often exhibit multiple phenotypes, and Shen *et al.* found that cisplatin and etoposide induced neuroendocrine differentiation (NED) in NSCLC cells similar to that in prostate cancer, and that targeting PRMT5 acted as a key factor in this process, which can synergistically kill cancer cells.[14]

To date, various strategies have been developed to overcome chemotherapy resistance.[15–17] However, many of these approaches significantly alter the pharmacokinetics of therapeutic agents and may induce toxicity in normal tissues. To address these limitations, a wide range of nanomaterials have been engineered to enhance treatment efficacy against chemo-resistant tumors.[18,19] Some of these nanoplatforms are designed to exploit the unique characteristics of the tumor microenvironment (TME), enabling responsive and precise therapeutic interventions.[20] More recently, sono-immunotherapy has emerged as a promising modality, offering tumor-specific cytotoxic effects by combining sonodynamic therapy with immune activation.[21–24] Mesoporous silica nanoparticles (MSNs) are often designed for controlled release of drugs due to their good biocompatibility and surface modification, among other characteristics.[25–27] The design concept is based primarily on external stimuli and internal responses, including pH, enzymes, light, redox and magnetic fields.[28–31] In order to achieve these stimulus-responsive properties, the main strategies include selecting suitable materials to act as 'gatekeepers' for the drug-carrying MSNs, binding them to the MSNs by physical adsorption or covalent attachment, and opening or closing them in response to specific stimuli to achieve drug release.[32,33] Oxidized hyaluronic acid used was used as a gating molecule *via* Schiff base reaction, and the acid tumor microenvironment caused the imine bond to be broken thus resulting in good pH-responsive properties and showed good inhibition of tumor cell proliferation.[34] Chen *et al.* designed a mesoporous nanocarrier with chitosan as a gating molecule, which can shed upon nucleophilic attack by GSH and restores charge transfer properties to trigger drug release.[35] Currently, the ideal drug delivery system in cancer therapy is designed to transport the drug precisely to the site of action for its release into action, avoiding premature release to other tissues and organs, which may cause damage to surrounding tissues and organs. Therefore, the targeted delivery of drugs to tumor cells or tissues through nanosystems can be used to mitigate side effects and improve drug efficacy.[36,37] To achieve this effect, the usual strategy is to combine nanomaterials with targeted ligands, including folic acid, RGD peptides, hyaluronic acid, *etc.*[38–40] Among these ligands, hyaluronic acid, due to its good biocompatibility and ability to bind specifically to the CD44 receptor highly expressed on the surface of various tumor cells, including non-small cell lung cancer.[41]

Based on this, we designed a mesoporous silica-based system for simultaneous targeted delivery of shRNA and anti-cancer drugs. The system consists of polyethyleneimine-modified mesoporous silica nanoparticles and methacryloylated hyaluronic acid hydrogel. Methacryloylated hyaluronan can bind to the CD44 receptor, which is highly expressed on the surface of cancer cells, and has good targeting ability.[42] Considering that PRMT5 is a potential oncogene and its upregulation is closely associated with multiple processes in cancer cells, we used shRNA of PRMT5 co-delivered with cisplatin to enhance the therapeutic effect. The synthesised nanomaterials and hyaluronic acid gel were characterised by a variety of techniques, and subsequently the release profiles of the nanomaterials were investigated under different conditions, and the endocytosis effect of the nanoparticles was examined using fluorescence microscopy. The anti-tumor effect of the composites on the drug-resistant cells was investigated by CCK8 cytotoxic assay, which demonstrated that the composite nanomaterials encapsulating cisplatin and PRMT5-shRNA have the function of targeting and removing drug-resistant lung cancer cells (NED cells or NED-like cells) (Scheme 1).

2 Materials and methods

2.1 Materials

Cetyltrimethylammonium bromide (CTAB, Sigma-Aldrich, 99%), tetraethyl silicate (TEOS, Merck, 98%),

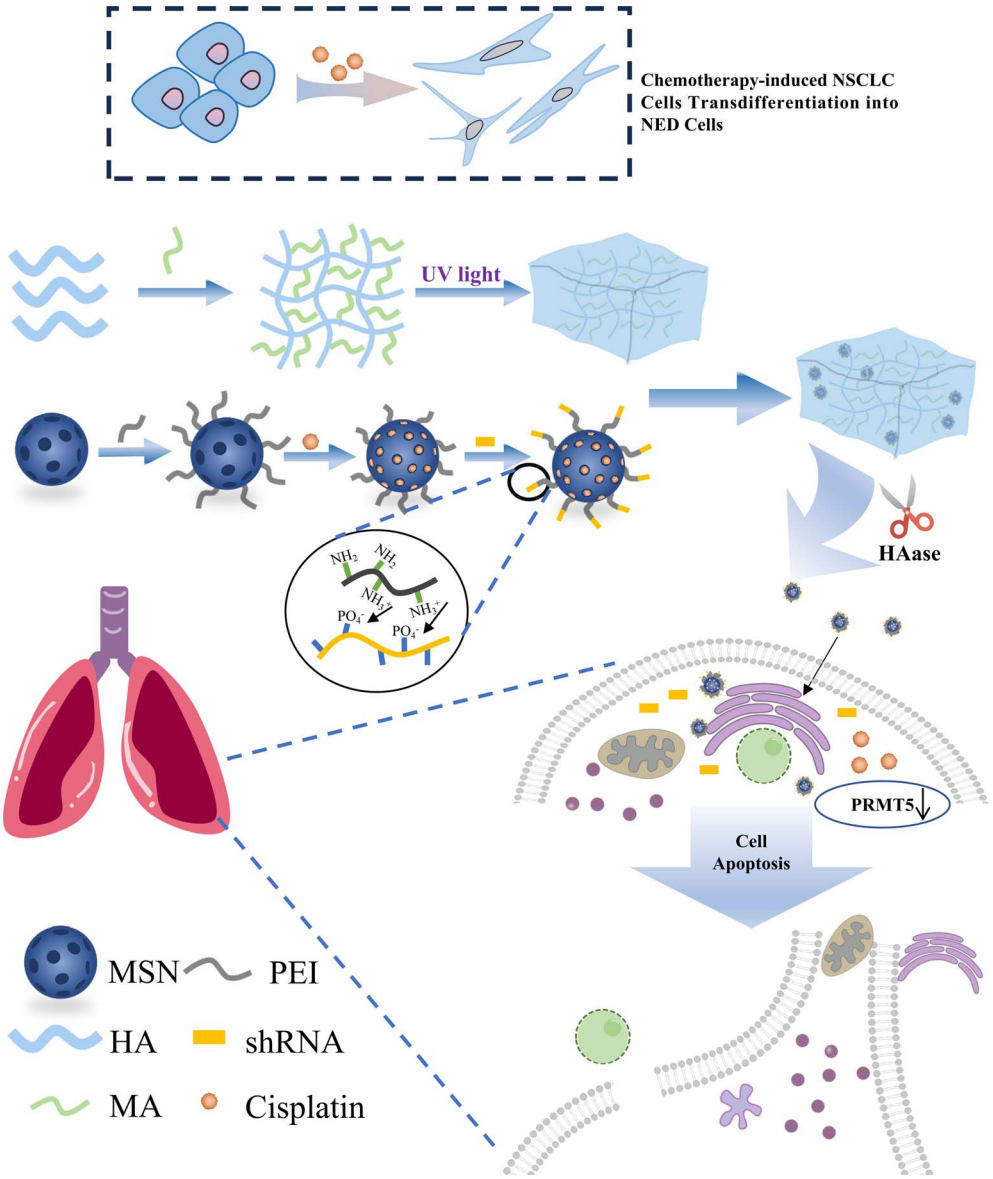

Scheme 1 Schematic illustration of chemotherapy-induced neuroendocrine differentiation (NED) in NSCLC cells and the subsequent therapeutic approach to eliminate chemotherapy-resistant NED-like cells *via* an enzyme-responsive hydrogel system co-delivering cisplatin and PRMT5 shRNA using mesoporous silica nanoparticles.

polyethyleneimine (PEI, Aladdin, 100 g, 99%), rhodamine B (RhB, Adamas, 100 g), sodium hyaluronate (HA, Macklin, M_w 100 000–200 000), methacrylic anhydride (MA, Adamas, 100 mL, 94%+), cisplatin (CDDP, Apexbio, 100 mg, 98%), *N*-hydroxybutanediimide (NHS, Adamas, 100 g, 99%), 1-ethyl-(3-dimethylaminopropyl)carbodiimide (EDC, Adamas, 100 g, 98%), tristoluene (Adamas, 100 mL, 99%+), PC9 cells, fetal bovine serum (FBS, Gibco, 500 mL), DMEM medium (Gibco, 500 mL), penicillin streptomycin solution (100×, Beyotime), TRI Reagent (Sigma).

2.2 shRNA construction

The PRMT5 target sequence (CCCATCCTCTTCCCTATTAAG), derived from The RNAi Consortium (TRC) TRCN0000303447, was cloned into the pLKO.1-copGFP-Puro vector (Synbio Technologies), which contains a strong enhanced green fluorescence protein (GFP) for visualization.

2.3 Cell culture

To induce drug resistance, 3×10^5 cells were seeded in 6 cm dishes containing DMEM supplemented with 10% fetal bovine serum, 100 U per mL penicillin, 100 μg per mL streptomycin, and incubated at 5% CO_2. When cell confluency reached 70–80%, the medium was replaced with fresh DMEM containing cisplatin at a final concentration of 3 μM. After 48 hours, the medium was replaced with cisplatin-free medium. This treatment cycle was repeated to establish cisplatin-resistant cells. The IC_{50} of drug-resistant cells was assessed using the CCK-8 assay, and the resistance index (RI) was calculated as the ratio of the IC_{50} of drug-resistant cells to that of parental cells.[43]

2.4 Preparation of mesoporous silica and MSN–PEI

Mesoporous silica nanoparticles (MSNs) were synthesized *via* the sol–gel method. Briefly, ammonia solution (25–28 wt%) was added to 1 L of ultrapure water, adjusted to pH 11, and heated to 50 °C. After dissolving 1.12 g of cetyltrimethylammonium bromide (CTAB) by stirring for 1 hour, 5.8 mL of tetraethyl orthosilicate (TEOS) was slowly added, and the mixture was reacted for 2 hours before overnight aging. The resulting precipitate was collected by centrifuged at 12 000 rpm for 5 min and washed thoroughly with water and ethanol. After a 4 day hydrothermal treatment at 140 °C, the precipitate was washed again, and CTAB was removed *via* refluxing in hydrochloric acid–ethanol solution at 70 °C for 36 hours. The purified mesoporous silica particles were obtained by centrifuge, washing and freeze-drying.

For polyethyleneimine (PEI) modification, 12.5 mg of MSNs were dispersed in water, followed by dropwise addition of 25 mg of PEI solution. The mixture was stirred for 30 minutes, washed, and the MSN–PEI particles were obtained *via* freeze-drying.

2.5 Drug encapsulation and release

Cisplatin (10 mg) was dissolved in 10 mL of deionized water, followed by the addition of 1 mL of MSN–PEI dispersion (1 mg mL^{-1}). The mixture was stirred in the dark for 18 hours, and the resulting solid was collected by centrifugation. The precipitate was dispersed in anhydrous ethanol, centrifuged at 12 000 rpm, and freeze-dried under vacuum. The drug loading capacity of the nanoparticles was then subsequently determined using ICP-MS. For release studies, the prepared composite hydrogel samples were immersed in phosphate-buffered saline (PBS) at pH 6.8 or 7.4 containing hyaluronidase (HAase, 50 U mL^{-1}), and incubated with shaking at 37 °C. The cumulative release of cisplatin was quantitatively determined by measuring the absorbance at 219 nm. The encapsulation efficiency and loading efficiency were calculated according to the formula:

$$\text{Encapsulation efficiency (\%)} = \frac{\text{(mass of drug released from the MSN)}}{\text{total mass of drug initially added}} \times 100\%$$

$$\text{Loading efficiency (\%)} = \frac{\text{(mass of drug released from the MSN)}}{\text{total mass of the carrier}} \times 100\%$$

2.6 Agarose gel retardation assay

The binding efficiency of shRNA to MSN–PEI was evaluated by combining 0.1 μg of plasmid with varying amounts of MSN–PEI (0.1–20 μg) and performing electrophoresis in 1% TAE buffer at 100 V for 30 min.

2.7 Preparation of HA-MA

Hyaluronic acid (HA, 1 g) was dissolved in 100 mL of ultrapure water under constant stirring, and the pH was adjusted to 8–9 using 5 mol per L NaOH. Methacrylic anhydride (MA, 1.6 mL) was added dropwise while maintaining the reaction in a 4 °C water bath. The pH was monitored and adjusted periodically to maintain consistency, and the solution was stirred overnight at 4 °C. Following the reaction, the mixture was dialyzed for 4 days against ultrapure water using a dialysis membrane with a molecular weight cutoff (MWCO) of 3.5 kDa, with water exchanged every 4 hours. The final HA-MA product was obtained through vacuum freeze-drying.

2.8 Preparation of mesoporous silica composite hydrogel

Hyaluronic acid-methacrylate (HA-MA, 10 mg) was dissolved in 5 mL of deionized water under stirring until fully dissolved, while mesoporous silica nanoparticles functionalized with polyethyleneimine (MSN–PEI, 10 mg) were dispersed in 1 mL of deionized water. To activate the carboxyl groups of HA-MA, 100 μL of EDC solution (48.8 mg mL^{-1}) and 100 μL of NHS solution (11.5 mg mL^{-1}) were added dropwise to the HA-MA solution and stirred for 15 min. Subsequently, the MSN–PEI dispersion was added to the HA-MA solution, and the reaction was allowed to proceed overnight. Following the reaction, the composite hydrogel was dialyzed against deionized water using a dialysis membrane with a molecular weight cutoff (MWCO) of 3.5 kDa for 24 h. The final mesoporous silica composite hydrogel was obtained through vacuum freeze-drying.

2.9 Cellular uptake of composite hydrogel

Rhodamine B was employed as a model drug to evaluate the cellular uptake behavior of the hydrogel. Rhodamine B emits red fluorescence upon cellular uptake, enabling analysis of the composite hydrogel's cellular internalization by comparing its fluorescence with that of nuclei stained with Hoechst 33258. A549-NED and PC9-NED cells were seeded in 6-well plates at a density of 2×10^5 cells per well and incubated overnight under standard culture conditions. Subsequently, the cells were treated with the composite hydrogel at a 10% volume fraction and co-cultured for 48 h. After incubation, the cells were washed three times with PBS, followed by staining with Hoechst 33258 solution (10 μg mL^{-1}) at room temperature for 15 min. The stained cells were visualized and imaged using a fluorescence microscope.

2.10 RT-qPCR

Total RNA was extracted using TRI Reagent (Sigma, USA). The RNA concentration was determined and reverse transcription was performed using BeyoRT™ III cDNA First Strand Synthesis Mix. Real-time quantitative PCR (qPCR) was performed using SYBR Green Master Mix (Beyotime) on the QX96M Real-Time PCR System. The primers used were described in Table 1.

2.11 Cytotoxicity assay

The cytotoxicity of the nanocomplexes to NED cells (NED-like cells) was assessed using the CCK-8 assay. Cells were seeded in 96-well plates at a density of 8×10^3 cells per well, and after 24 hours, the culture medium was replaced with DMEM containing various nanocomplex formulations. For the preparation

Table 1 Primers for qPCR

Gene	Forward (5′–3′)	Reverse (5′–3′)
PRMT5	CAAATGCCGTGGTGACGCTA	ATGGGAGCCAGAAAGGAAGT
GAPDH	TGAGTACGTCGTGGAGTCCA	CAGGAGGCATTGCTGATGATC
MDR1	TTCATTTTGGTGCCTGGCAG	CTGACAGTCCAAGAACAGGA
BCRP	TAATGGAGATTCCACTGCTG	TGGTGTAGCTGATCTCCTTG

of the different formulations, serum-free DMEM was first prepared and then diluted to the desired concentration using complete medium. The formulations tested included CDDP, PRMT5-shRNA, NC-shRNA, HA-MA, CDDP@MSN–PEI + PRMT5-shRNA, and HA + CDDP@MSN–PEI + PRMT5-shRNA, with CDDP concentrations ranging from 1 to 11 μM. The cytotoxicity of composite hydrogel at different concentrations on normal cells (BEAS-2B) was also tested to determine the selective action of hydrogel on lung cancer cells. After 72 hours of incubation, 10 μL of CCK-8 solution was added to each well, and absorbance was measured at 450 nm. Cell viability was calculated based on the absorbance values.

2.11.1 Cell apoptosis analysis. Cell apoptosis was evaluated using Annexin V-FITC/PI double staining followed by flow cytometry. Transdifferentiated human non-small cell lung cancer cells (induced by CDDP), PC9-NED and A549-NED, were seeded into 6-well plates under 37 °C, 5% CO_2 overnight. The next day, cells were assigned to five treatment groups including the negative control group, hydrogel (HA-MA) group, CDDP group (medium containing CDDP), nanoparticle group (medium containing CDDP@MSN–PEI + PRMT5 nanoparticles) and composite hydrogel group (HA-MA + CDDP@MSN–PEI + PRMT5). After 72 hours of incubation, cells were harvested and stained with Annexin V-FITC and propidium iodide (PI) according to the manufacturer's instructions. The stained cell suspensions were immediately analyzed by flow cytometry.

2.11.2 Statistical analysis. Experiments were performed in triplicate, and the data were presented as the mean ± standard deviation (SD). Statistical analysis was performed using two-way analysis of variance (ANOVA) followed by Tukey's post-hoc test for pairwise comparisons, with significance levels set at $*P < 0.05$, $**P < 0.01$, and $***P < 0.001$.

3 Result and discuss

3.1 Cell induction

Firstly, PC9 cells and A549 cells were induced to undergo transdifferentiation by gradually increasing the cisplatin concentration, resulting in the generation of NED-like cells. NED-like cells are defined as the longest neuronal protrusions, which are at least twice the length of the cell body diameter.[44] Two weeks post-induction, the NED-like cells were clearly observed. The number of NED-like cells was quantified using ImageJ. The production rates of NED-like cells observed to be 26.37% and 19.74% in PC9 and A549 cells, respectively (Fig. 1a and b). Curve fitting using GraphPad Prism revealed that the IC_{50} value for PC9 cells was 3.952 μmol L^{-1}, whereas the IC_{50} value for PC9-NED cells was 14.57 μmol L^{-1}, yielding a resistance index of approximately 3.84. The IC_{50} values for A549 cells and A549-NED cells were 5.261 μmol L^{-1} and 11.91 μmol L^{-1}, respectively, with a resistance index of 2.26 (Fig. 1c), consistent with the characteristics of drug-resistant cell lines.

3.2 Preparation of mesoporous silica and MSN–PEI

Before preparing the composite hydrogel, mesoporous silica and PEI–MSN were prepared. TEM of mesoporous silica is shown in Fig. 2a, which reveals uniformly spherical particles with a distinct mesoporous structure and an average particle size of approximately 200 nm. After PEI modification, the particle size increased from 216.6 nm to 285.9 nm, as shown in the DLS plot, and the zeta potential shifted from −0.33 mV to 46.21 mV due to the large positive charge of PEI (Fig. 2b and c). Energy dispersive X-ray spectroscopy (EDS) results in Fig. 2d show that the PEI-modified mesoporous silica exhibits

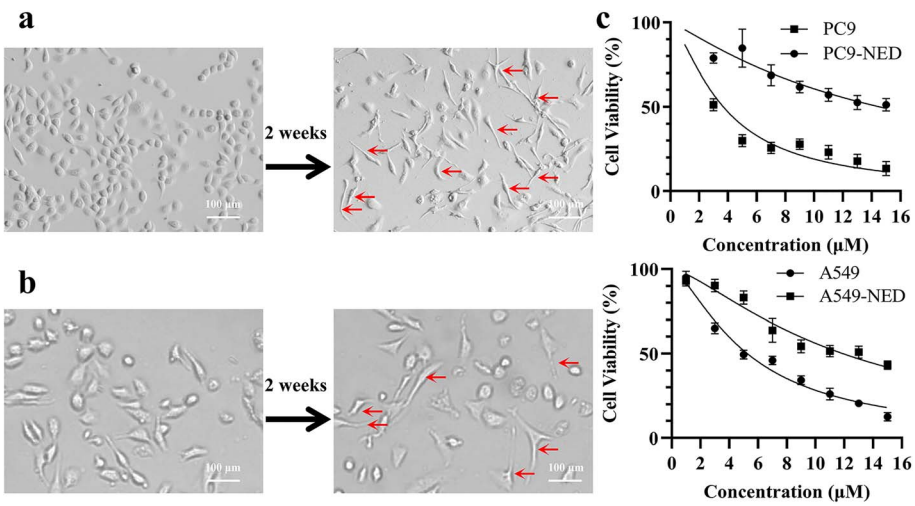

Fig. 1 Neuroendocrine differentiation of non-small cell lung cancer cells induced by cisplatin (NED-like cells were indicated by red arrows). (a) PC9 cells. (b) A549 cells. (c) Comparison of cytotoxicity before and after NED induction.

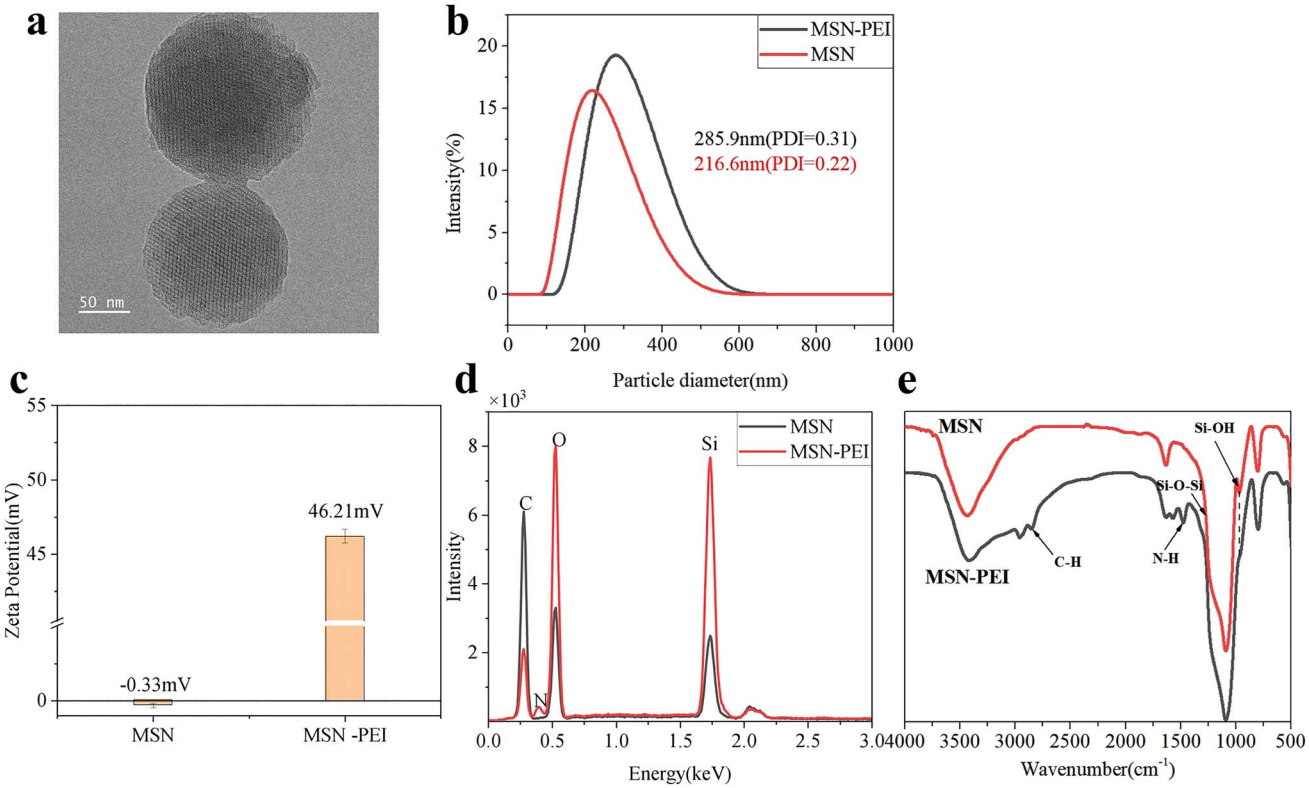

Fig. 2 Synthesis of MSN–PEI nanoparticles. (a) Transmission electron microscopy (TEM) images of mesoporous silica (MSN). (b) Dynamic light scattering (DLS) analysis of MSN–PEI. (c) Zeta potential of the MSN and MSN–PEI nanoparticles. (d) Energy dispersive X-ray spectroscopy (EDS) analysis of MSN and MSN–PEI. (e) FTIR spectra of MSN and MSN–PEI.

characteristic nitrogen peaks, confirming successful MSN–PEI preparation. FTIR spectra revealed C–H and N–H vibration at 2580 cm^{-1} and 1473 cm^{-1}, respectively, in the PEI-modified MSN particles (Fig. 2e).

3.3 Preparation of HA-MA

To confirm the successful grafting of HA-MA, ^{1}H-NMR and FTIR were used for characterization. As shown in Fig. 3a, new peaks appeared at 5.6 and 6.1 ppm, corresponding to the protons on

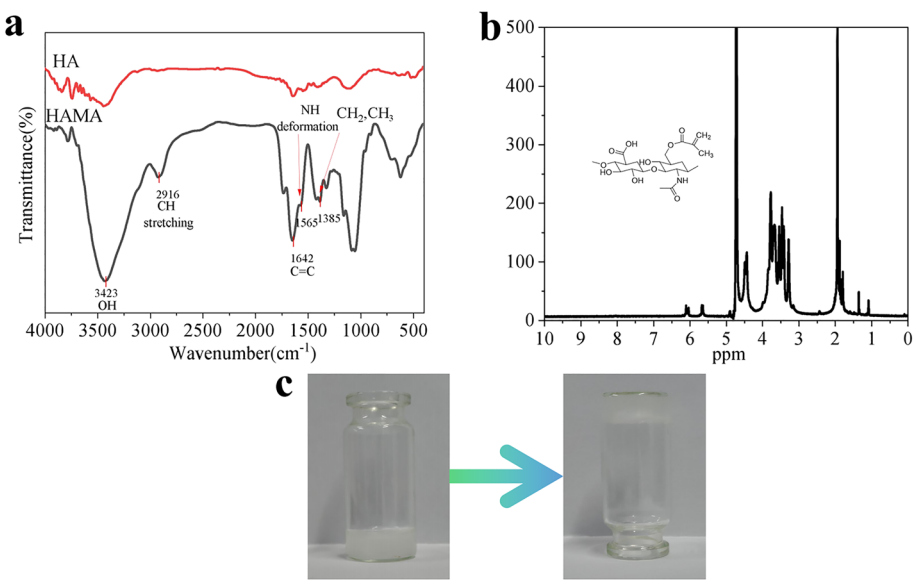

Fig. 3 Synthesis of HA-MA. (a) FTIR spectra of HA and HA-MA. (b) ^{1}H NMR spectra of methacryloylated hyaluronic acid (HA-MA). (c) Sol–gel transition and hydrogel formation.

the methacrylic acid olefins, compared to the original HA. The proton peaks at 3–4 ppm represent signals from the 10 protons in the HA backbone, while the peaks at 1.8 ppm correspond to the protons on the methyl methacrylate groups, and the peaks at 1.9 ppm correspond to the protons on the *N*-acetyl group of the HA backbone.

The FTIR spectra (Fig. 3b) show that in HA, the absorption bands at 3120–3564 cm^{-1} are attributed tointra- and intermolecular hydrogen bonding from O–H and N–H stretching vibrations. The band at 2928 cm^{-1} corresponds to the asymmetric and symmetric stretching of C–H, while the COO^- stretching vibration is observed at 1398 cm^{-1}. The bands at 1620, 1538, and 1458 cm^{-1} correspond to the C=O stretching vibration of the amide C=O stretching vibration of amide I band, N–H bending vibration of amide II band, and the C–H vibration of amide III band, respectively. Additionally, a C=C double bond peak at 1642 cm^{-1} was observed in HA-MA, conforming the successful synthesis of HA-MA. The HA-MA hydrogel can be crosslinked under UV light, transitioning from sol to gel, which is visually observable (Fig. 3c).

3.4 Drug encapsulation and release

In this study, we initially evaluated the drug loading efficiency of the nanoparticles, followed by a simulation of the hydrogel's swelling behavior in a tumor-mimicking environment. We further assessed the drug release profiles under normal physiological conditions and in the presence of hyaluronidase. Modification of MSNs with polyethyleneimine (PEI) significantly enhanced their drug encapsulation efficiency and drug loading capacity, possibly due to coordination interactions between PEI and the drug. The encapsulation efficiency and drug loading capacity of MSN–PEI reached 78.60% ± 0.21% and 34.70% ± 0.75%, respectively, compared with 58.26% ± 0.18% and 31.53% ± 0.63% for unmodified MSNs. The swelling rate of the hydrogel in a slightly acidic environment reached approximately 40% after 84 hours (Fig. 4a). This swelling was primarily due to hydrogen bonding between the hydrophilic groups and water molecules, as well as the interaction between the crosslinked network and water, both of which contributed to the expansion. We hypothesize that this swelling behavior enhances drug release by providing more space for drug diffusion. Additionally, the results showed that in the absence of hyaluronidase, drug release was minimal, with only about 10% of the drug being released. In contrast, the presence of hyaluronidase significantly increased drug release efficiency, with approximately 60% of the drug released after 144 hours (Fig. 4b). This enhancement release was attributed to both the increased space created by hydrogel swelling and the hydrogel degradation induced by hyaluronidase, which created a more favorable environment for drug release.

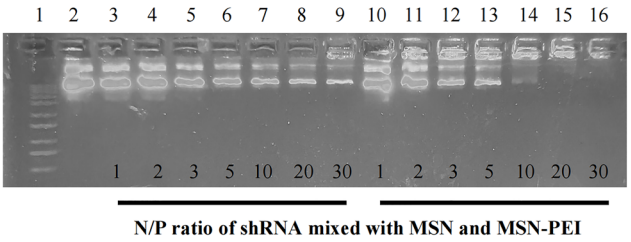

Fig. 5 Agarose gel retardation of MSN and MSN–PEI after incubation with different concentrations of shRNA (plasmid).

3.5 Agarose gel retardation assay

The loading capacity of MSN–PEI for shRNA (plasmid) was evaluated using an agarose gel retardation assay. As shown in Fig. 5, lane 1 contained the DNA marker, lane 2 showed free shRNA, lanes 3–9 displayed shRNA complexes with MSN at various weight ratios (1 : 1, 1 : 2, 1 : 3, 1 : 5, 1 : 10, 1 : 20, 1 : 30), and lanes 10–16 showed shRNA complexes with MSN–PEI at corresponding ratios (1 : 1, 1 : 2, 1 : 3, 1 : 5, 1 : 10, 1 : 20, 1 : 30). The migration rate of shRNA decreased progressively as the MSN–PEI to shRNA ratio increased. At a 20 : 1 ratio and above, shRNA was fully retained in the wells. In contrast, the migration of shRNA mixed with MSN alone was unaffected, likely due to the protonated amino groups on MSN–PEI, which enhanced its proton-sponge effect and binding affinity for shRNA.

3.6 Cellular uptake

Cellular uptake is a crucial indicator of the biological properties of hydrogel materials. *In vitro* cellular uptake experiments were

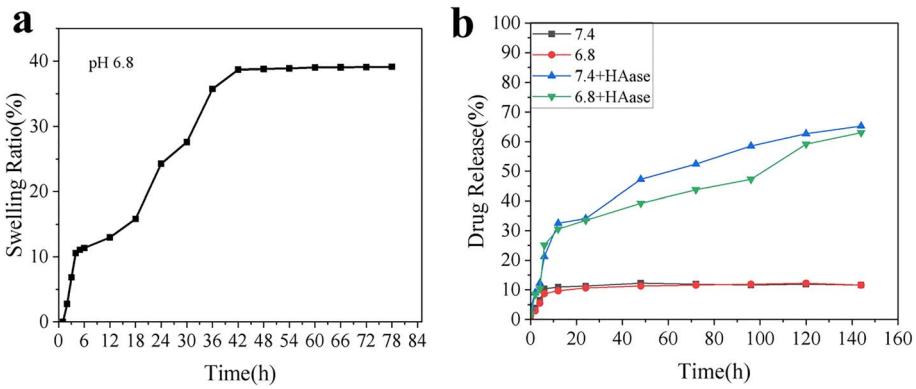

Fig. 4 Drug encapsulation and release profile. (a) Swelling behavior of the hydrogel in PBS (pH 6.8). (b) Drug release kinetics of the hydrogel in simulated environment.

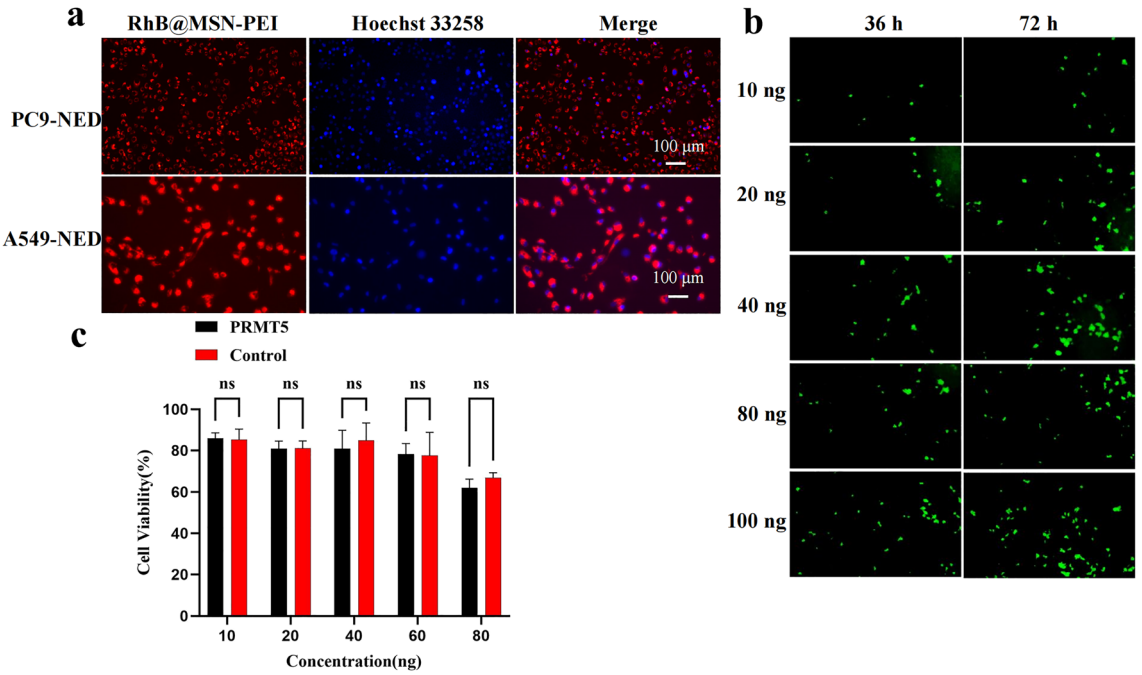

Fig. 6 Cellular uptake and cytotoxicity evaluation. (a) Uptake of the hydrogel by PC9-NED and A549-NED cells, visualized by rhodamine B (red) and nuclear staining (blue). (b) Green fluorescence indicating successful gene delivery by MSN–PEI/shRNA complexes, with increasing intensity over time and concentration. (c) Cytotoxicity analysis of MSN–PEI/shRNA complexes at various concentrations, showing minimal toxicity.

conducted using cisplatin-induced PC9 and A549 cells. Hydrogel leachate containing Rhodamine B (RhB)-encapsulated MSN–PEI nanoparticles was added to the Petri dishes to simulate the drug release process. Cellular uptake of the nanoparticles was observed after 48 hours. As shown in Fig. 6a, both cell lines exhibited strong red fluorescence from rhodamine B and blue fluorescence from the stained nuclei. This is attributed to the positive charge on the surface of MSN–PEI, which facilitates binding to the negatively charged cell membrane, thereby enhancing nanoparticle uptake. Following transfection with the MSN–PEI/shRNA complex, a gradual increase in the green fluorescence signal was observed over time and with increasing concentration, indicating successful nanoparticle uptake and expression of the delivered gene sequences (Fig. 6b). Additionally, cytotoxicity assays demonstrated low toxicity of MSN–PEI/shRNA to the cells, suggesting that MSN–PEI alone has limited efficacy in targeting drug-resistant tumor cells (Fig. 6c).

3.7 *In vitro* cytotoxicity

To assess the effects of these materials on chemotherapy-resistant non-small cell lung cancer (NSCLC) cells, the CCK-8 assay was used to evaluate the survival rates of PC9-NED and A549-NED cells treated with CDDP@MSN–PEI/shRNA. The experimental groups included CDDP, PRMT5-shRNA, NC-shRNA, HA-MA, and HA-MA + CDDP@MSN–PEI/PRMT5-shRNA. The CDDP concentration was set at 1, 3, 5, 7, 9, and 11 μmol L^{-1}, while the mass ratio of nanoparticles to shRNA was fixed at 30 : 1. The results showed that the cytotoxicity of all treatment groups increased with increasing concentration. No significant differences were observed between the NC group and cells treated with shRNA alone. Notably, the cytotoxicity of the HA-MA + CDDP@MSN–PEI/PRMT5-shRNA group was significantly stronger than that of the CDDP group, indicating that the nanoparticles enhanced cisplatin uptake (Fig. 7a and b). Moreover, the cytotoxicity in this group was higher than that in the HA-MA + CDDP@MSN–PEI/NC-shRNA group, suggesting that PRMT5 inhibition significantly enhanced the sensitivity of drug-resistant cells to cisplatin. The RT-qPCR results confirmed effective silencing of PRMT5 and downregulation of drug resistance-related genes *MDR1* and *BCRP* following delivery of PRMT5-shRNA *via* the HA-MA + CDDP@MSN–PEI/PRMT5-shRNA hydrogel (Fig. 7c–e). In addition, the HA-MA + CDDP@MSN–PEI/PRMT5-shRNA hydrogel exhibited reduced cytotoxicity toward normal cells, indicating a preferential uptake by lung cancer cells (Fig. 7d).

3.8 Cell apoptosis analysis

The apoptotic activity of various treatment groups against NED-like non-small cell lung cancer (NSCLC) cells was analyzed and quantified by flow cytometry (Fig. 8). Among all groups, the hydrogel formulation loaded with therapeutic agents exhibited the most pronounced pro-apoptotic effect on NED-like cells. Notably, since the NED phenotype was induced with cisplatin (CDDP) prior to each experiment, the resulting NED-like cell populations displayed some instability compared to established drug-resistant cell lines. Although some cell loss occurred during sample preparation, likely due to detachment of non-adherent cells following treatment, the HA-MA + CDDP@MSN–PEI/PRMT5-shRNA hydrogel group consistently

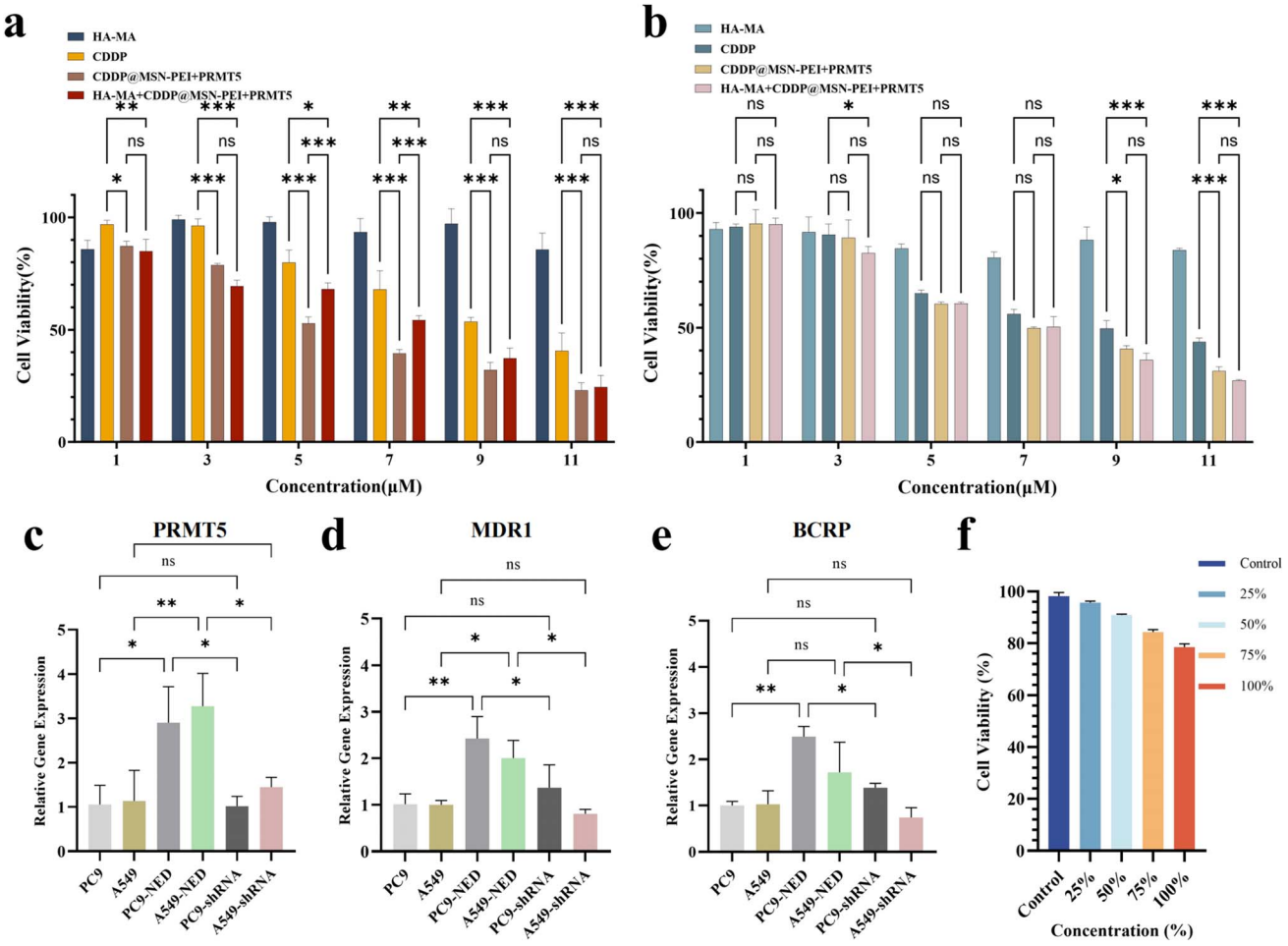

Fig. 7 Cell viability and gene expression analysis in NED-like NSCLC cells and normal bronchial epithelial cells following various treatments. (a) Cell viability of PC9-derived NED-like cells after treatment. (b) Cell viability of A549-derived NED-like cells after treatment. (c–e) Relative mRNA expression levels of PRMT5, MDR1, and BCRP in NED-like NSCLC cells following treatment with HA-MA + CDDP@MSN–PEI/PRMT5-shRNA, indicating effective PRMT5 silencing and modulation of drug resistance genes. (f) Cell viability of normal bronchial epithelial cells (BEAS-2B) after exposure to the extract of HA-MA + CDDP@MSN–PEI/PRMT5-shRNA hydrogel. * means $P < 0.05$, ** means $P < 0.01$, *** means $P < 0.001$.

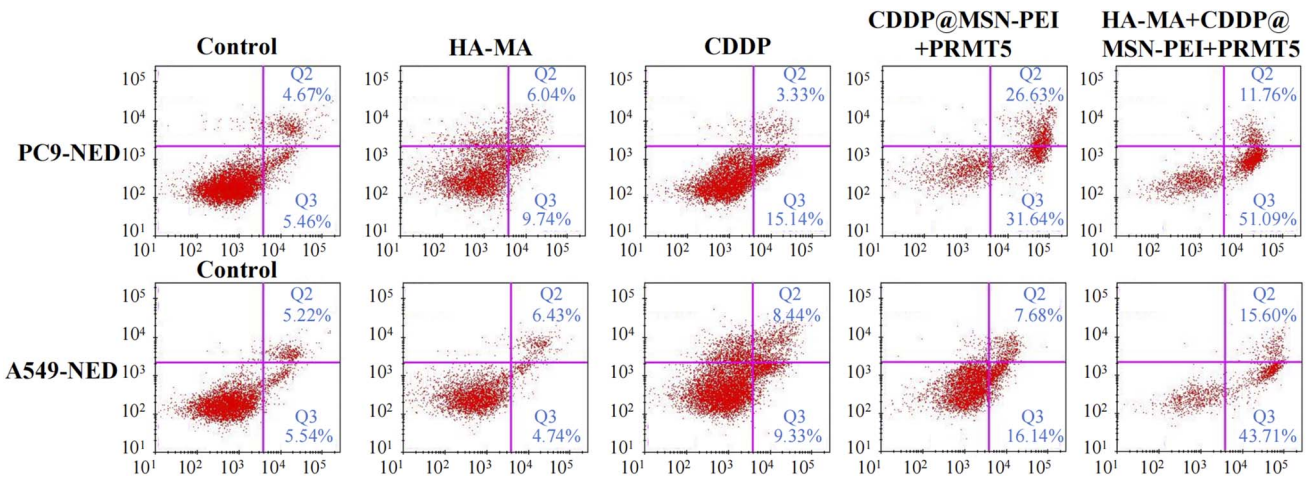

Fig. 8 Apoptotic activity in NED-like NSCLC cells following various treatments, as assessed by flow cytometry. Q2 represents late apoptotic cells. Q3 represents early apoptotic cells. The percentage of apoptotic cells (early and late) was quantified to evaluate the therapeutic efficacy of each treatment.

exhibited a pronounced induction of apoptosis, highlighting its strong therapeutic potential.

4 Conclusion

In conclusion, this study presents an innovative enzyme-responsive hydrogel system functionalized with mesoporous silica nanoparticles (MSN) for the co-delivery of shRNA and cisplatin, aimed at overcoming drug resistance in non-small cell lung cancer (NSCLC) cells, particularly those exhibiting neuroendocrine differentiation (NED). This system was engineered by coating the MSN surface with polyethyleneimine (PEI) to enable efficient binding of negatively charged shRNA, followed by functionalization with methacryloylated hyaluronic acid (HA-MA) for targeted delivery. Cisplatin was encapsulated within the mesopores of the MSN, while the PEI coating facilitated the binding of shRNA, creating a synergistic platform for drug and gene delivery.

The HA-MA modification enables selective targeting of CD44 receptors, which are overexpressed on the surface of NSCLC NED-like cells, ensuring efficient delivery to the tumor cells and minimizing off-target effects. *In vitro* release profiles demonstrated that this composite system enables controlled release in conditions mimicking the tumor microenvironment, such as the slightly acidic pH (6.8) and the presence of hyaluronidase, which is highly active in tumor tissues. This dual-trigger mechanism enhances the precision and efficiency of both drug and gene delivery.

Biocompatibility assays confirmed that the hydrogel composite is safe for healthy cells, ensuring minimal toxicity while providing effective tumor-targeted therapy. Cellular uptake studies showed that the composite material was efficiently internalized by cancer cells, confirming the potential of this system to overcome cellular barriers in drug-resistant NSCLC NED-like cells. Cytotoxicity assays demonstrated that the PRMT5-shRNA component effectively silenced PRMT5 expression, a key protein associated with drug resistance and tumor progression. This silencing resulted in sensitizing the NSCLC NED-like cells to cisplatin, significantly improving therapeutic efficacy compared to cisplatin treatment alone.

These results suggest that MSN-based hydrogel composites offer a promising approach for overcoming drug resistance in NSCLC NED-like cells. The combination of targeted gene therapy and chemotherapy within a single system provides a powerful tool to reverse resistance mechanisms and enhance cisplatin efficacy in resistant cancer cells. By silencing key genes like PRMT5, the system not only overcomes resistance but also enhances the therapeutic potential of cisplatin, making it more effective in combating resistant tumor cells.

This work lays the groundwork for the development of advanced drug and gene delivery platforms that can be tailored to address the challenges of drug resistance in NSCLC, especially in the NED phenotype. Future studies will focus on further optimizing this hydrogel system for clinical application, including *in vivo* validation and investigation of its therapeutic potential across different stages of NSCLC and other types of cancer. The combination of precise, enzyme-responsive drug release and gene silencing offers a highly promising strategy for overcoming drug resistance in NSCLC NED-like cells, providing a new avenue for effective cancer therapy.

Data availability

The authors confirm that the data supporting the findings of this study are available within the article.

Author contributions

Yi Liu: writing – review & editing, visualization, supervision, funding acquisition, resources, project administration, methodology, conceptualization. Zheng Zhang: investigation, validation, visualization, data curation, formal analysis, writing – original draft. Huyang Du: investigation, validation, visualization. Xiangjun Chen: investigation, validation, visualization. Nan Hu: investigation, project administration. Tingting Yu: investigation, project administration. Meili Hou: investigation, project administration. Xiaolin Yu: project administration, methodology, funding acquisition.

Conflicts of interest

The authors declare no conflict of interest.

Acknowledgements

This work was supported by the Foundation of Zigong Academy of Big Data and Artificial Intelligence in Medical Science (2024-YGY-01-01, 2023-YGY-1-04 and 2022ZCYGY02), the Natural Science Foundation General Program of Sichuan (2022NSFSC0363 and 2022NSFSC0810), and the Medical Science Research Project of Sichuan (S20076).

References

1 J. Kryczka, *et al.*, Molecular Mechanisms of Chemoresistance Induced by Cisplatin in NSCLC Cancer Therapy, *Int. J. Mol. Sci.*, 2021, **22**(16), 8885.
2 H. Y. Min and H. Y. Lee, Mechanisms of resistance to chemotherapy in non-small cell lung cancer, *Arch. Pharmacal Res.*, 2021, **44**(2), 146–164.
3 Y. Xiao, F. T. Lin and W. C. Lin, ACTL6A promotes repair of cisplatin-induced DNA damage, a new mechanism of platinum resistance in cancer, *Proc. Natl. Acad. Sci. U. S. A.*, 2021, **118**(3), e2015808118.
4 L. Wang, *et al.*, The Role of Tumour Metabolism in Cisplatin Resistance, *Front. Mol. Biosci.*, 2021, **8**, 691795.
5 Y. Abe, *et al.*, PRMT5-mediated methylation of STAT3 is required for lung cancer stem cell maintenance and tumour growth, *Commun. Biol.*, 2024, **7**(1), 593.

6 X. Sheng and Z. Wang, Protein arginine methyltransferase 5 regulates multiple signaling pathways to promote lung cancer cell proliferation, *BMC Cancer*, 2016, **16**, 567.
7 Y. Chen, *et al.*, Targeting protein arginine methyltransferase 5 in cancers: Roles, inhibitors and mechanisms, *Biomed. Pharmacother.*, 2021, **144**, 112252.
8 X. Sheng, N. Bowen and Z. Wang, GLI pathogenesis-related 1 functions as a tumor-suppressor in lung cancer, *Mol. Cancer*, 2016, **15**, 25.
9 J. Huang, *et al.*, PRMT5 Promotes EMT Through Regulating Akt Activity in Human Lung Cancer, *Cell Transplant.*, 2021, **30**, 9636897211001772.
10 S. Zhang, *et al.*, Targeting PRMT5/Akt signalling axis prevents human lung cancer cell growth, *J. Cell. Mol. Med.*, 2019, **23**(2), 1333–1342.
11 M. Li, *et al.*, The arginine methyltransferase PRMT5 and PRMT1 distinctly regulate the degradation of anti-apoptotic protein CFLAR(L) in human lung cancer cells, *J. Exp. Clin. Cancer Res.*, 2019, **38**(1), 64.
12 H. Zhou, *et al.*, PRMT5 activates KLF5 by methylation to facilitate lung cancer, *J. Cell. Mol. Med.*, 2024, **28**(5), e17856.
13 J. L. Owens, *et al.*, PRMT5 Cooperates with pICln to Function as a Master Epigenetic Activator of DNA Double-Strand Break Repair Genes, *iScience*, 2020, **23**(1), 100750.
14 Q. Shen, *et al.*, PRMT5 promotes chemotherapy-induced neuroendocrine differentiation in NSCLC, *Thorac. Cancer*, 2023, **14**(18), 1764–1773.
15 K. K. W. To, *et al.*, Utilizing non-coding RNA-mediated regulation of ATP binding cassette (ABC) transporters to overcome multidrug resistance to cancer chemotherapy, *Drug Resistance Updates*, 2024, **73**, 101058.
16 L. Su, *et al.*, Targeting Src reactivates pyroptosis to reverse chemoresistance in lung and pancreatic cancer models, *Sci. Transl. Med.*, 2023, **15**(678), eabl7895.
17 Y. Wang, *et al.*, Overcoming cancer chemotherapy resistance by the induction of ferroptosis, *Drug Resistance Updates*, 2023, **66**, 100916.
18 X. Zheng, *et al.*, Nanomedicine Combats Drug Resistance in Lung Cancer, *Adv. Mater.*, 2024, **36**(3), e2308977.
19 Z. Y. Han, *et al.*, Inhalable Capsular Polysaccharide-Camouflaged Gallium-Polyphenol Nanoparticles Enhance Lung Cancer Chemotherapy by Depleting Local Lung Microbiota, *Adv. Mater.*, 2023, **35**(38), e2302551.
20 Y. Liu, *et al.*, A dual-responsive hyaluronic acid nanocomposite hydrogel drug delivery system for overcoming multiple drug resistance, *Chin. Chem. Lett.*, 2022, 107583.
21 J. Cai, *et al.*, Defect Engineering of Biodegradable Sulfide Nanocage Sonozyme Systems Enables Robust Immunotherapy Against Metastatic Cancers, *Adv. Funct. Mater.*, 2024, **34**(52), 2411064.
22 B. Geng, *et al.*, Single Atom Catalysts Remodel Tumor Microenvironment for Augmented Sonodynamic Immunotherapy, *Adv. Mater.*, 2024, **36**(25), e2313670.
23 B. Geng, *et al.*, Near-infrared phosphorescent carbon dots for sonodynamic precision tumor therapy, *Nat. Commun.*, 2022, **13**(1), 5735.
24 Y. Wang, *et al.*, A heterojunction-engineering nanodrug with tumor microenvironment responsiveness for tumor-specific cuproptosis and chemotherapy amplified sono-immunotherapy, *Biomaterials*, 2025, **321**, 123319.
25 D. Tarn, *et al.*, Mesoporous silica nanoparticle nanocarriers: biofunctionality and biocompatibility, *Acc. Chem. Res.*, 2013, **46**(3), 792–801.
26 A. Slita, *et al.*, Characterization of modified mesoporous silica nanoparticles as vectors for siRNA delivery, *Asian J. Pharm. Sci.*, 2018, **13**(6), 592–599.
27 Y. Feng, *et al.*, Mesoporous Silica Nanoparticles-Based Nanoplatforms: Basic Construction, Current State, and Emerging Applications in Anticancer Therapeutics, *Adv. Healthcare Mater.*, 2023, **12**(16), e2201884.
28 Z. Zhang, *et al.*, pH-sensitive and bubble-generating mesoporous silica-based nanoparticles for enhanced tumor combination therapy, *Acta Pharm. Sin. B*, 2021, **11**(2), 520–533.
29 A. Llopis-Lorente, *et al.*, Enzyme-Powered Gated Mesoporous Silica Nanomotors for On-Command Intracellular Payload Delivery, *ACS Nano*, 2019, **13**(10), 12171–12183.
30 J. Fan, *et al.*, Photo-responsive degradable hollow mesoporous organosilica nanoplatforms for drug delivery, *J. Nanobiotechnol.*, 2020, **18**(1), 91.
31 F. Zhang, *et al.*, Coordination and Redox Dual-Responsive Mesoporous Organosilica Nanoparticles Amplify Immunogenic Cell Death for Cancer Chemoimmunotherapy, *Small*, 2021, **17**(26), e2100006.
32 A. García-Fernández, *et al.*, New Advances in In Vivo Applications of Gated Mesoporous Silica as Drug Delivery Nanocarriers, *Small*, 2020, **16**(3), e1902242.
33 P. Díez, *et al.*, Ultrafast Directional Janus Pt-Mesoporous Silica Nanomotors for Smart Drug Delivery, *ACS Nano*, 2021, **15**(3), 4467–4480.
34 X. Enyu, *et al.*, Construction and performance evaluation of pH-responsive oxidized hyaluronic acid hollow mesoporous silica nanoparticles, *Int. J. Biol. Macromol.*, 2024, **257**(Pt 1), 128656.
35 Y. Chen, *et al.*, Chitosan-Gated Fluorescent Mesoporous Silica Nanocarriers for the Real-Time Monitoring of Drug Release, *Langmuir*, 2020, **36**(24), 6749–6756.
36 A. Kanungo, C. Mohanty and S. Acharya, Smart Cancer Nanomedicine for Synergetic Therapy, *Curr. Med. Chem.*, 2025, **32**(2), 286–300.
37 V. Jeannot, *et al.*, Anti-tumor efficacy of hyaluronan-based nanoparticles for the co-delivery of drugs in lung cancer, *J. Controlled Release*, 2018, **275**, 117–128.
38 X. Sun, *et al.*, Folic Acid and PEI Modified Mesoporous Silica for Targeted Delivery of Curcumin, *Pharmaceutics*, 2019, **11**(9), 430.
39 J. Zhang, *et al.*, Multifunctional envelope-type mesoporous silica nanoparticles for tumor-triggered targeting drug delivery, *J. Am. Chem. Soc.*, 2013, **135**(13), 5068–5073.
40 S. Li, *et al.*, Microneedle Patches with Antimicrobial and Immunomodulating Properties for Infected Wound Healing, *Adv. Sci.*, 2023, **10**(22), e2300576.

41 F. Alsaikhan, Hyaluronic acid-empowered nanotheranostics in breast and lung cancers therapy, *Environ. Res.*, 2023, **237**(Pt 1), 116951.
42 D. Bhattacharya, *et al.*, Impact of structurally modifying hyaluronic acid on CD44 interaction, *J. Mater. Chem. B*, 2017, **5**(41), 8183–8192.
43 M. McDermott, *et al.*, In vitro Development of Chemotherapy and Targeted Therapy Drug-Resistant Cancer Cell Lines: A Practical Guide with Case Studies, *Front. Oncol.*, 2014, **4**, 40.
44 Y. Chen, *et al.*, Erk/MAP kinase signaling pathway and neuroendocrine differentiation of non-small-cell lung cancer, *J. Thorac. Oncol.*, 2014, **9**(1), 50–58.